Fast-Track SCAL Methodology for Evaluating Relative Permeability in CO_2 Storage Aquifers

Fabrice Pairoys[1,*], *Maria* Villalobos[2]

[1]SLB Reservoir Laboratories, 6350 West Sam Houston Parkway North, Houston, TX 77041, United States
[2]Lapis Carbon Solutions, 5420 LBJ Freeway, Bldg. 2, Suite 1330, Dallas, TX 75240, United States

Abstract. Geological storage of CO_2 in deep saline formations is becoming a key strategy for climate change mitigation, providing a safe and long-term method to reduce atmospheric emissions. The success of this approach depends on the characteristics of both the reservoir rock and the caprock. For the reservoir, storage capacity and fluid mobility are critical, while for the caprock, effective sealing to prevent upward migration of injected CO_2 is essential. The SCAL experimental program, designed to quantify fluid mobility through relative permeability (K_r) tests and determine threshold entry pressure (P_{ce}) using standard methods, may not be completed before the Class VI permit application deadline. Therefore, an initial expedited approach is sometime required to deliver dynamic reservoir modeling in support of the permitting process. This study addresses the time constraints by delivering critical data within a compressed timeframe. Core plugs were first analyzed for porosity and permeability to establish rock typing. Each representative sample was then divided into two sections: one for mercury intrusion capillary pressure (MICP) testing and the other for dynamic entry pressure measurement, not reported in this study. CO_2–brine interfacial tension (σ) and contact angle (θ) were measured to convert MICP-derived capillary pressure (P_c) values. This paper describes the methodology for inferring the primary drainage relative permeabilities from capillary pressure using the Brooks–Corey model. The imbibition CO_2 relative permeability was estimated using Land's model under the assumption of water-wet conditions and no hysteresis in brine relative permeability. This accelerated workflow enabled delivery of the Kr data within less than two weeks, ahead of the permit application deadline. Upon completion of the full SCAL program, the rapid relative permeability approach was benchmarked against core flooding experiments conducted under reservoir conditions to ensure that the expedited methodology yields a "sufficiently accurate" initial relative permeability dataset. The results of this study indicate that the inferred MICP-derived Kr curves offer an acceptable proxy for estimating CO_2–brine relative permeability in primary drainage, a finding further corroborated by dynamic numerical simulations at the reservoir scale.

1 Introduction and Bibliography

Capillary pressure (P_c) and relative permeability (K_r) data are essential for modeling CO_2 migration in reservoir dynamic simulations because they govern multiphase displacement, storage efficiency, and saturation front evolution. Accurate prediction requires high-quality SCAL laboratory measurements, accounting for hysteretic effects, and rigorous data conditioning.

Unfortunately, good quality Special Core Analysis (SCAL) data, especially from the laboratory core flooding tests, may take too long to be acquired. In some cases, SCAL data results may not be fully available before a class VI permit application deadline. This application is required in the United States to drill and operate wells for the permanent underground storage of CO_2.

Permitting authorities will not grant authorization to inject until obtaining a robust 3D simulation of the CO_2 plume: without K_r and P_c curves, the models cannot accurately predict how fast the CO_2 will move. This is reason why the K_r and P_c curves, obtained from a well-designed laboratory SCAL program, are mandatory for the successful completion of the technical review.

When the SCAL program is not completed before the audit, other methods are required to provide K_r and P_c:

a) Use of analogs, requiring limited core and fluid analyses from the reservoir where the CO_2 could be injected for storage,

b) Digital rock physics, again requiring limited reservoir core and fluid analyses, but it will also require core scanning using micro-CT scanner,

c) Indirect approaches from data that can be quickly acquired such as porosity ϕ, permeability K, capillary pressure P_c from MICP, and basic fluid analysis.

* Corresponding author: fpairoys@slb.com

Method c) was used in this study to develop a robust workflow to generate consistent relative permeability and capillary pressure curves for dynamic CO_2-injection simulations in deep saline formations (e.g., the injection zone under investigation in this study is located within the Mount Simon Sandstone). The approach reduces uncertainty, ensures internal consistency, and reliably represents primary drainage and imbibition processes under reservoir conditions relevant to long-term CO_2 storage.

This workflow establishes a structured methodology for generating synthetic saturation functions to support CO_2-injection simulations in the Mount Simon Sandstone prior to the availability of final laboratory-measured capillary pressure and relative permeability data. The primary stages of the workflow are summarized below:

1. Reservoir flow-unit characterization,
2. Drainage capillary-pressure characterization, including,
   - Core sample selection Mercury Injection Capillary Pressure (MICP up to 60,000 psi on 1” by 1” samples) test,
   - Capillary pressure conversion to reservoir conditions,
3. Derivation of drainage relative-permeability curves from MICP data,
4. Integration of Special Core Analysis (SCAL) Data,
5. Dynamic simulation results using synthetic and measured relative permeability inputs,
6. Impact of Imbibition Capillary Pressure on Dynamic Simulation Incorporating Measured Imbibition P_c.

Nevertheless, this workflow misses some important components: the endpoints. The main question is how to properly scale the K_r curve between a representative saturation range and K_r endpoint values without experimental measurements.

This point is addressed in the following section: a literature review on clay-free sandstone aquifers (as for the selected reservoir for CO_2 injection and storage) was conducted, providing a range of K_r endpoints to characterize the plume migration (primary drainage cycle) and for understanding the trapping capacity of the reservoir (imbibition cycle).

- **Primary Drainage K_r Endpoints**

The assessment of CO_2–brine primary drainage across various sandstone facies demonstrated that clean formations exhibit significantly higher gas mobility than historical models suggested, provided that experimental artifacts like capillary end effects are rigorously eliminated. [1], [2], [3] and [4] established that absolute permeability, rather than porosity, serves as the primary predictor for drainage endpoints. Their combined datasets show that as permeability improves from <10 mD to ~850 mD, irreducible water saturation (S_{wi}) typically drops from 0.65 to 0.15, while the maximum CO_2 relative permeability (K_{rg} Max) climbs from 0.05 to 0.80. This highlights that while mineralogy and minor clay content can increase brine retention, the structural connectivity of the pore network remains the dominant control on CO_2 flow capacity.

In the moderate permeability range (approx. 10 to100 mD), studies by [5] and [6] using NMR and CT imaging on San Saba and Mount Simon sandstones identified S_{wi} values between 0.30 and 0.45. They noted that even in nearly pure quartz matrices, CO_2 can induce a shift toward a weakly water-wet state, which, combined with diverse pore-size distributions, explains why gas endpoints often remain significantly below unity. Conversely, for exceptionally clean, high-permeability media (>1,000 mD) such as Bentheimer and Fontainebleau, [7], [8] and [9] reported highly efficient drainage with S_{wi} as low as 0.05 and K_{rg} Max reaching 0.95, serving as a theoretical benchmark for maximum injectivity in ideal saline aquifers.

These fundamental trends are corroborated by the work of [10], [11], and [12], who demonstrated that eliminating capillary heterogeneity in the viscous limit consistently yields K_{rg} Max values exceeding 0.85 in high-K rocks. Further validation of the transition to lower Swi near the 1,000 mD threshold is provided by [13] and [14]. Recent industrial benchmarks from the Northern Lights project and major operators ([15], [16]., [17]) confirm these ranges for North Sea reservoirs, where S_{wi} typically stabilizes between 0.18 and 0.30 and K_{rg} Max converges between 0.40 and 0.70 when using standardized, representative SCAL protocols.

Based on the above references, with converging results, Table 1 is generated to provide primary drainage CO_2-Brine relative permeability endpoints for clean sandstones, categorized by permeability range.

Table 1. CO_2-Brine primary drainage K_r endpoints per permeability range.

K Range	S_{wi} (frac.)	K_{rg} Max
<10 mD	0.40-0.65	0.05-0.25
10-100 mD	0.30-0.45	0.20-0.50
100-500 mD	0.25-0.40	0.30-0.60
500-1000 mD	0.15-0.25	0.55-0.80
>1000 mD	0.05-0.20	0.60-0.95

- **Imbibition K_r Endpoints**

Like the primary drainage, the assessment of CO_2–brine imbibition is fundamental for quantifying residual trapping capacity in saline aquifers. [3] and [4] demonstrated that imbibition curves in clean sandstones become more linear as interfacial tension decreases, leading to higher total relative mobility. [18] and [19] further established that residual gas saturations (S_{gr}) typically range from 13% to 92%, depending on the maximum initial gas saturation reached during drainage, a relationship fundamentally modeled using Land's model [20].

This trapping behavior is considered an inherent rock property that remains stable across varying reservoir pressures and temperatures ([21]), though it is sensitive to the rock's pore-body-to-throat ratio and coordination number ([22]). While sandstones are initially strongly water-wet, [5] used NMR to confirm that exposure to CO_2 can shift the system toward a weakly water-wet state by reducing hydrophilicity ([23]), which can impact the re-imbibition efficiency. Furthermore, hysteretic effects lead to a significant reduction in CO_2 relative permeability during imbibition compared to the drainage cycle ([24]), a trend that is particularly pronounced at higher injection pressures in low-permeability media ([25]).

Based on the literature review, ranges of K_r endpoints for imbibition are reported in Table 2.

Table 2. CO2-Brine imbibition K_r endpoints per permeability range.

K Range	S_{gr} (frac.)	K_{rw} Max
<10 mD	0.10-0.25	0.05-0.15
10-100 mD	0.15-0.30	0.10-0.25
100-500 mD	0.20-0.40	0.15-0.40
500-1000 mD	0.25-0.45	0.30-0.60
>1000 mD	0.30-0.50	0.50-0.85

To conclude this literature review, large variations of endpoint values are observed for both primary drainage and imbibition cycles.

There are many other references that confirm the ranges indicated in Table 1 and Table 2, all based on experimental SCAL programs. But these programs may be time consuming and experimentally challenging for quantifying fluid mobility through relative permeability (K_r) tests using standard methods (steady-state, unsteady-state, semi-dynamic): the entire program may not be completed before the Class VI permit application deadline.

In our study, the K_r curves were quickly and indirectly obtained using MICP P_c and Brooks-Corey approach [26], with corrected P_c curves using IFT and contact angle measured with equilibrated CO_2 and brine at reservoir conditions. With the endpoints being unknown, we provide in this paper a workflow to un-normalize the indirect K_r curves.

2 Reservoir Rock and Fluid Properties

The deep saline formation considered for CO_2 injection/storage is a Lower Mount Simon sandstone (>94% quartz, <3% total clay), containing three main flow units that were defined using MICP porosity-permeability and using reservoir quality index RQI calculation. They are qualified as high, mid, and low flow units with:

a) RQI<0.25 for the low flow unit
b) 0.25≤RQI≤1.0 for the mid flow unit
c) RQI>1.0 for the high flow unit

The equilibrated CO_2-brine IFT and CO_2-brine-rock contact angle were measured at reservoir conditions (104°F of temperature, 1732 psi of pressure). These data were required to convert the air-mercury Pc from the MICP tests (Table 3).

Table 3. IFT and contact angle values.

Fluid System	Test conditions	IFT (dyne/cm)	Contact angle (°)
Air-Hg	ambient	485	130
CO_2-Brine	reservoir	22.4	43.1

After having measured MICP, IFT and contact angle values, the samples were classified according to the RQI ranges. Table 4 reports the results of 9 MICP samples used to generate average capillary pressure curves of each flow unit.

Table 4. Core samples selected for each flow unit obtained from MICP.

Flow Unit	Sample ID	ϕ (frac.)	K (mD)	RQI
High	50	0.13	356	1.62
	31	0.12	421	1.86
	56	0.21	398	1.35
Mid	27	0.17	58.6	0.58
	26	0.14	21.6	0.39
	24	0.15	55.6	0.60
Low	25	0.11	1.50	0.12
	15	0.08	1.24	0.12
	11	0.13	1.20	0.10

In addition to the fast MICP/IFT/contact angle measurements, three core flooding tests were initiated on composite stacks, with one core flooding test representing the mid flow unit (stack 1), and two core flooding tests representing the high flow unit (stack 2 and stack 3). Due to its unfavorable properties, the reservoir zone identified as low flow unit case was not considered for CO_2 injection.

Each stack was composed of 4 core plugs (Langaas arrangement). The intrinsic properties of each stack are reported in Table 5.

Table 5. Routine core analysis results for each stack.

Stack Id	Flow Unit	ϕ (frac.)	K_w (mD)	RQI
Stack 1	Mid	0.143	24.90	0.41
Stack 2	High	0.213	370.8	1.31
Stack 3	High	0.224	1118	2.21

The brine permeability K_w values at 100% brine saturation are used as reference permeabilities to compute the relative permeabilities Kr.

3 K_r Curves from MICP

Figure 1 represents the air-mercury P_c curves of the 9 samples listed in Table 4. The Leverett J-function from [27] is then used to average the capillary pressure curves per flow unit.

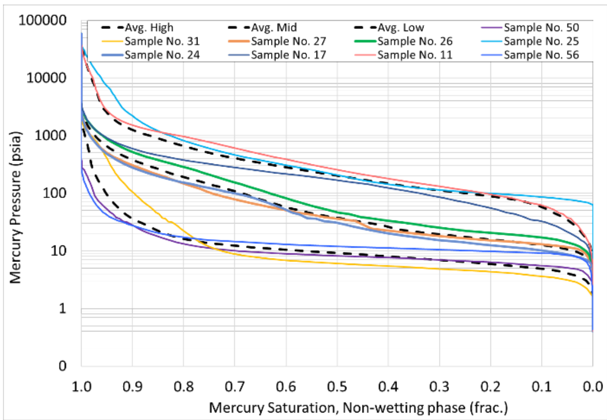

Fig. 1. MICP P_c curves and average P_c curves per flow unit.

The air-mercury Pc curves are then converted to CO_2-brine P_c curves using IFT and contact angle values from Table 3.

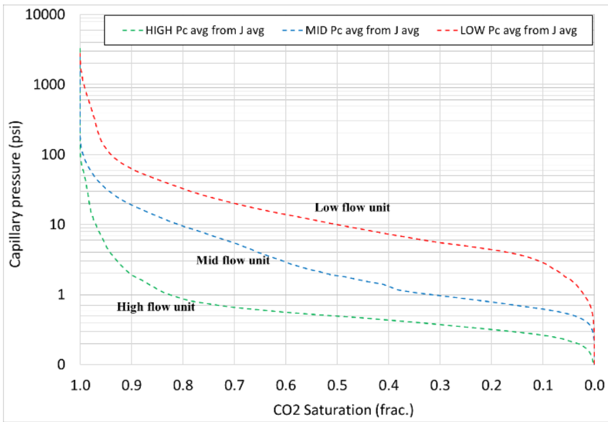

Fig. 2. CO_2-brine capillary pressure curves P_c (from MICP) for each flow unit.

Only the mid and high flow unit reservoir sections are considered for further CO_2 injection: there was no attempt to determine K_r curves from the low flow unit section.

The primary drainage relative permeability curves for the mid and high-flow units are derived from the CO_2–brine P_c curve using the approach described in [28]. For each flow unit, we:

a) Use the Brooks-Corey P_c equation 1 to fit the CO_2-brine P_c curves from Fig. 3 (log-log scale), providing the pore size distribution index λ.

$$P_c = P_{ce}(S_w^*)^{\frac{-1}{\lambda}} \qquad \text{Eq. 1}$$

With P_{ce} the entry capillary pressure and S_w^* the reduced water saturation.

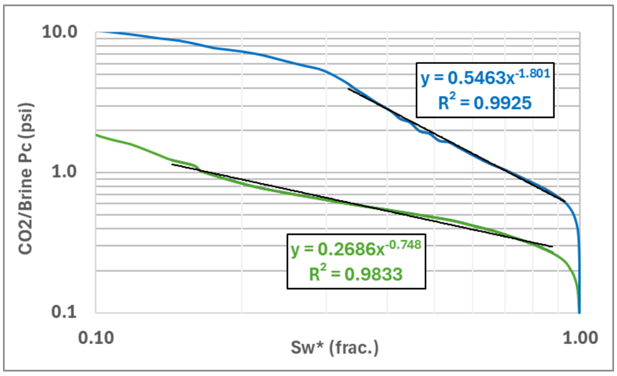

Fig. 3. Averaged CO_2-Brine P_c curves on log-log plot for λ determination, per flow unit (high flow unit in green, mid flow unit in blue).

b) Use the Brooks-Corey K_r equations 2 and 3, using the obtained λ values from a)

$$K_{rw} = S_w^{*\frac{(2+3\lambda)}{\lambda}} \qquad \text{Eq. 2}$$

$$K_{rg} = (1 - S_w^*)^2\left(1 - (S_w^*)^{\frac{(2+\lambda)}{\lambda}}\right) \qquad \text{Eq. 3}$$

At this stage, the saturation and K_r values vary from 0 to 1: realistic endpoints must be set. For the primary drainage cycle, Timur's equation 4 ([29]) and Bennion et Bachu's equation 5 ([4]) were used to calculate S_{wi} and K_{rg} max respectively.

$$S_{wi} = \frac{93\phi^{2.2}}{\sqrt{K}} \qquad \text{Eq. 4}$$

$$K_{rg}Max = 0.85(1 - S_{wi})^{2.5} \qquad \text{Eq. 5}$$

To calculate S_{wi} from Equation 4, average MICP porosity and MICP Swanson permeability, for each flow unit, were used. The results are reported in Table 6.

Table 6. Flow unit parameters

Flow Unit	ϕ (frac.)	K (mD)	λ	S_{wi} (frac.)	K_{rg} Max
High	0.151	389	0.87	0.07	0.70
Mid	0.160	45.3	0.56	0.25	0.42

The imbibition relative permeability curves are then determined by assuming that the rock remains strongly water-wet: in that case, there is no water relative permeability hysteresis (primary drainage and imbibition K_{rw} curves overlay). Regarding the CO_2 phase, it is considered as the non-wetting phase, exhibiting hysteresis. To calculate the CO_2 relative permeability K_{rg} the Land's model [20] is used (Equation 6 and Equation 7).

$$S_{gF}^* = \frac{1}{2}\left(S_g^* - S_{gr}^* + \sqrt{\left(S_g^* - S_{gr}^*\right)^2 + \frac{4}{C}\left(S_g^* - S_{gr}^*\right)}\right) \quad \text{Eq. 6}$$

$$K_{rg} = S_{gF}^*\left(1 - \left(1 - S_{gf}^*\right)^{\frac{2+3\lambda}{\lambda}-2}\right) \quad \text{Eq. 7}$$

Because the residual CO_2 saturation S_{gr} value is unknown, Table 2 can be used to provide estimated endpoints for each flow unit during the imbibition cycle, brine displacing CO_2. Nevertheless, the uncertainty was narrowed down by using S_{gr} value of 20% for both flow units, consistent with the measurements made by [7] and [8] on the same Mount Simon sandstone.

Table 7 reports the endpoints used to build the un-normalized K_r curves in primary drainage and imbibition.

Table 7. SCAL endpoints for each flow unit.

Flow Unit	S_{wi}	K_{rg} Max	S_{gr}
High	0.07	0.70	0.20
Mid	0.25	0.42	0.20

Because it is assumed there is no hysteresis on the wetting phase, i.e. brine, the K_{rw} Max values correspond to the value at S_{gr} on the primary drainage K_{rw} curve.

In the following sections, D1 and I1 correspond to the primary drainage and imbibition respectively. The K_r curves for mid and high flow units are shown in Figures 4 and 5.

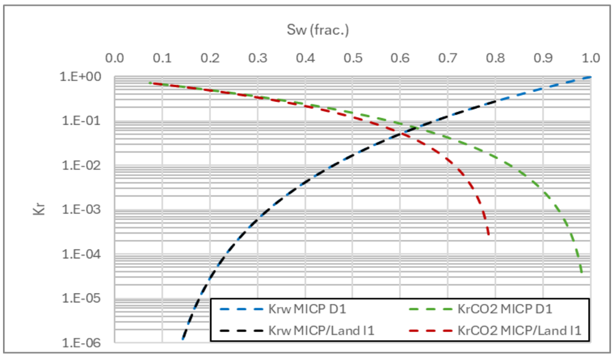

Fig. 4. Indirect MICP K_r curves for the high flow unit.

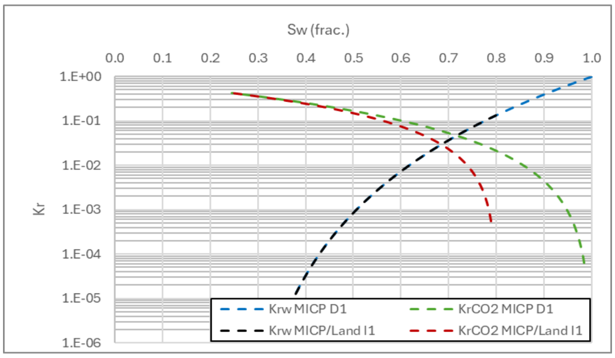

Fig. 5. Indirect MICP K_r curves for the mid flow unit.

This set of K_r curves were used for performing the reservoir simulations, to monitor the plume migration and assess the CO_2 trapping efficiency. The input Corey parameters for primary drainage and imbibition are listed in Table 8.

Table 8. Primary drainage D1 and Imbibition I1 Corey parameters for each flow unit.

High Flow Unit		
	D1	I1
S_{wi} (frac.)	0.074	0.074
S_{gr} (frac.)	0.00	0.20
K_{rg} Max	0.702	0.702
K_{rw} Max	1.000	0.279
N_w	5.25	5.25
N_{CO_2}	2.50	2.00
Mid Flow Unit		
S_{wi} (frac.)	0.245	0.245
S_{gr} (frac.)	0.00	0.20
K_{rg} Max	0.421	0.421
K_{rw} Max	1.000	0.135
N_w	6.50	6.50
N_{CO_2}	2.25	1.70

The resulting simulations, at the reservoir scale will be presented in the dynamic reservoir simulation section.

4 K_r Curves from Coreflooding Tests

Three coreflooding tests on composite stacks were then initiated:

- Stack 1 representing the mid flow unit, primary drainage and imbibition cycles
- Stack 2 and Stack 3 represent the high flow unit, primary drainage and imbibition cycles

Each stack was composed of 4 core plugs (Langaas arrangement, [30]). The intrinsic properties of each stack are reported in Table 5.

The unsteady-state coreflooding tests were performed at reservoir conditions (104°F of temperature, 1732 psi of pressure, 1660 psi of Net Confining Stress).

Viscosity and density of brine and CO_2 were measured at reservoir conditions (Table 9). At the reservoir conditions, CO_2 is under supercritical phase.

Table 9. Fluid properties at reservoir conditions

Fluid	Density (g/cc)	Viscosity (cP)
Brine	1.045	0.875
CO_2	0.698	0.057

The experimental SCAL program started right after RCA, MICP and fluid analysis. The K_r coreflooding results were not obtained before the audit. The results were used to validate the indirect approach.

For both primary drainage and imbibition cycles, brine or CO_2 productions (V_w or Vg), differential pressure (dP) and in situ saturation monitoring (ISSM) using a 1D x-ray scanner, were recorded. As recommended by [28], bump rates were only applied during the primary drainage: as a matter of fact, bump rates are not recommended during an imbibition cycle when dealing with CO_2, mainly due to compressibility issue impacting the saturation calculation via material balance. For the primary drainage cycle, 3 rates were applied, with the first, main rate approximating a low field rate (~1ft/day). For the imbibition cycle, only the low field rate was applied.

To determine the relative permeability K_r curves, history-match of the experimental data is performed using a 1D core analysis numerical software.

- **Stack 1 Results (Mid Flow Unit)**

Stack 1 represents the mid flow unit. Figures 6, 7, and 8 represent the experimental data and the history-match results of the primary drainage cycle.

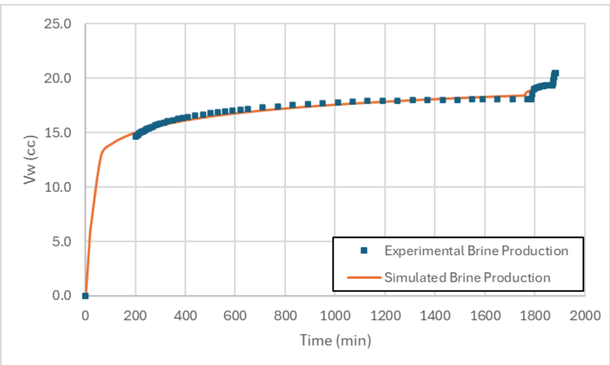

Fig. 6. Experimental and numerical primary drainage brine production, V_w.

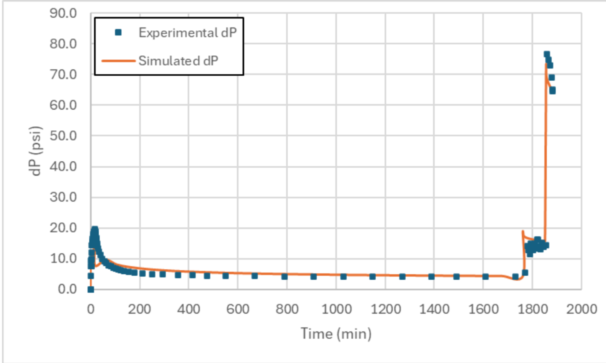

Fig. 7. Primary drainage experimental and numerical dP.

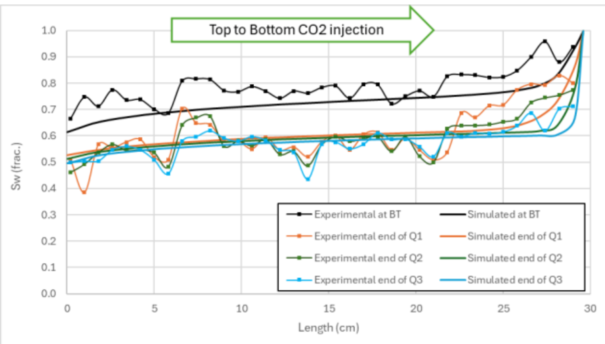

Fig. 8. Primary drainage experimental and numerical saturation profiles.

To succeed in history-matching the experimental data, K_r and P_c are tuned. The MICP-converted CO_2-brine P_c was used as first P_c guess for primary drainage. It was then tuned using the saturation profiles, especially the $Sw(P_c=0)$ value observed on the saturation profiles at the end of each applied CO_2 rates. The P_o magnitude and entry capillary pressure P_{ce} were also tuned using the Swanson equation ($P_o=6.24\phi/\sqrt{K}$) and the Leverett-J function for P_{ce} calculation.

Same approach was followed for the imbibition cycle (Figures 9, 10, 11).

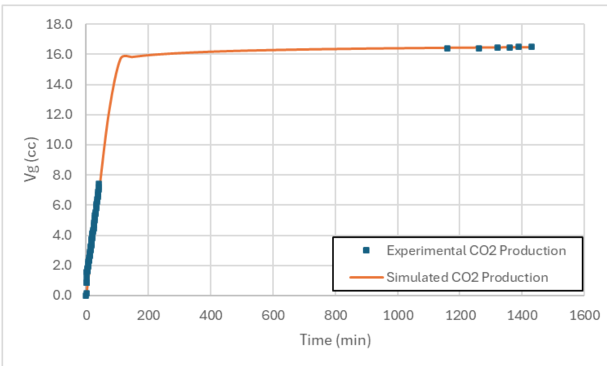

Fig. 9. Imbibition experimental and numerical CO_2 production Vg.

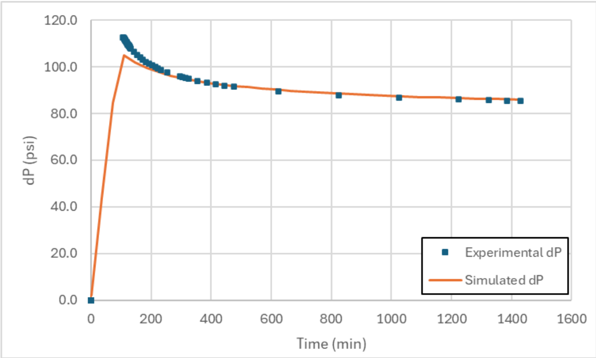

Fig. 10. Imbibition experimental and numerical dP.

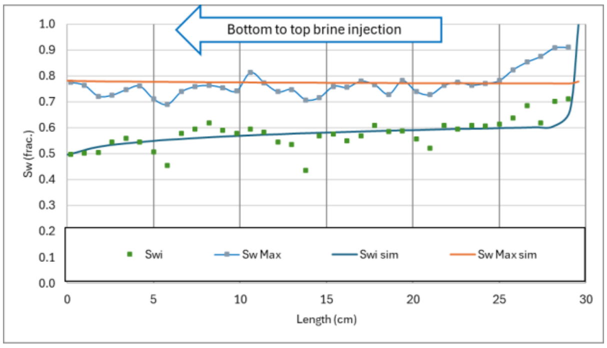

Fig. 11. Imbibition experimental and numerical saturation profiles.

The resulting K_r and P_c curves are shown in Figures 12 and 13.

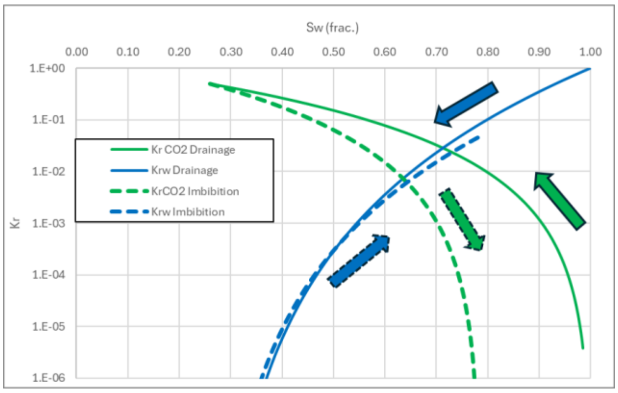

Fig. 12. Stack 1 K_r curves for the mid flow unit.

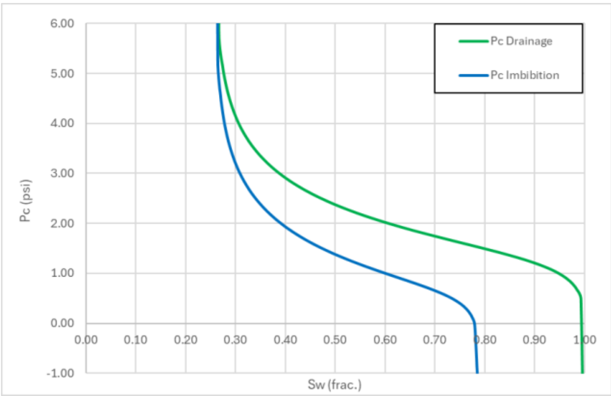

Fig. 13. Stack 1 P_c curve for the mid flow unit.

Figure 12 highlights a large hysteresis on the CO_2 non-wetting phase, while limited for the brine wetting phase.

Figure 13 represents the primary drainage and imbibition P_c curves used to better history-match the experimental data. Note that adding the imbibition P_c helped in improving the quality of the history-match (compared to simulation with P_c=0). The P_c curve is positive, confirming the strong water wetness of the rock.

Same process was applied to Stacks 2 and 3: in the following section, only the relative permeability K_r and P_c curves, post-history match, are presented.

- **Stack 2 Results (High Flow Unit)**

The quality of the history-match was as good as for Stack 1. The K_r and P_c curves are shown in Figures 14 and 15.

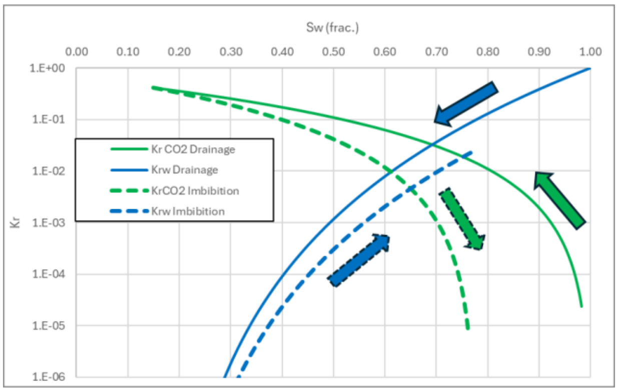

Fig. 14. Stack 2 K_r curves for the high flow unit.

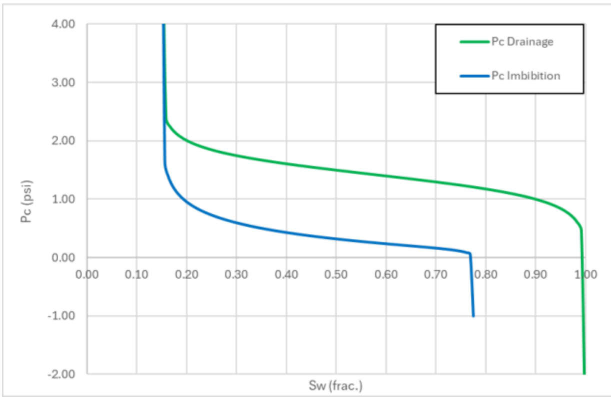

Fig. 15. Stack 2 P_c curve for the high flow unit.

Unlike stack 1, Figure 14 x highlights a slight hysteresis is on the brine phase, though it remains modest compared to the observed hysteresis on the CO_2 phase.

- **Stack 3 Results (High Flow Unit)**

As for the other stacks, the quality of the history-match was found to be good. The K_r and P_c curves are represented in Figures 16 and 17.

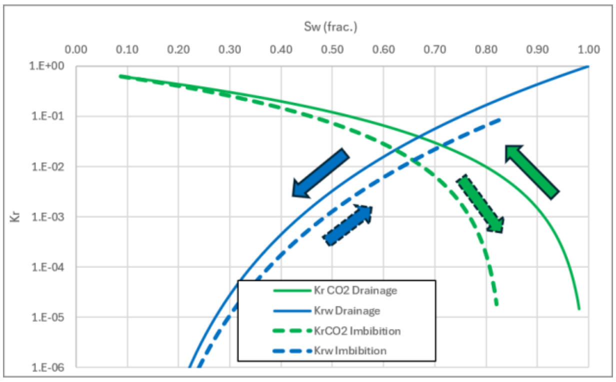

Fig. 16. Stack 3 K_r curves for the high flow unit.

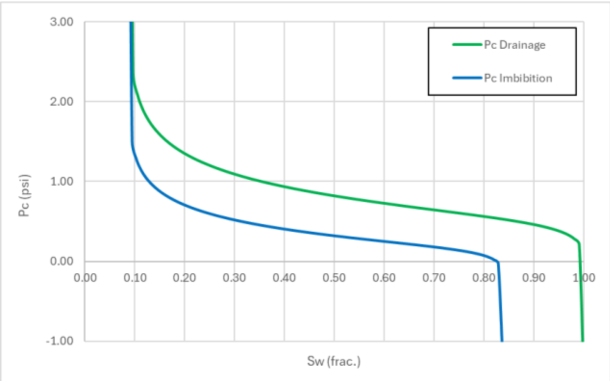

Fig. 17. Stack 3 P_c curve for the high flow unit.

Stack 3 behaves like stack 1: slight hysteresis on the brine phase, high hysteresis on the CO_2 phase, as expected.

Table 10 summarizes the primary drainage and imbibition K_r Corey parameters after the history-match for all stacks.

Table 10. Primary drainage D1 and Imbibition I1 K_r Corey parameters for each stack.

	Stack 1 Mid Flow Unit	Stack 2 High Flow Unit	Stack 3 High Flow Unit
Primary Drainage Cycle			
S_{wi} (frac.)	0.260	0.150	0.087
K_{rg} Max	0.502	0.422	0.629
N_w	7.26	7.62	7.21
N_{CO_2}	3.02	2.51	2.74
Imbibition Cycle			
S_{gr}	0.215	0.225	0.164
K_{rw} Max	0.049	0.025	0.093
N_w	6.51	7.62	7.21
N_{CO_2}	3.35	2.80	2.68

Note that the primary drainage cycle starts at water saturation S_w=100% and K_{rw} Max=1, while the initial conditions of the imbibition cycle correspond to the primary drainage endpoints.

The 3 experimental results were available more than 1 month after the audit. Nevertheless, these results are crucial to validate the indirect method: the experimental K_r curves can be compared to those obtained from MICP.

5 Comparison between indirect and experimental methods

Stack 1 vs MICP Mid Flow Unit:

Figures 18, and 19 show the comparison between the indirect and lab-measured K_r and fractional flow F_w curves for Stack 1.

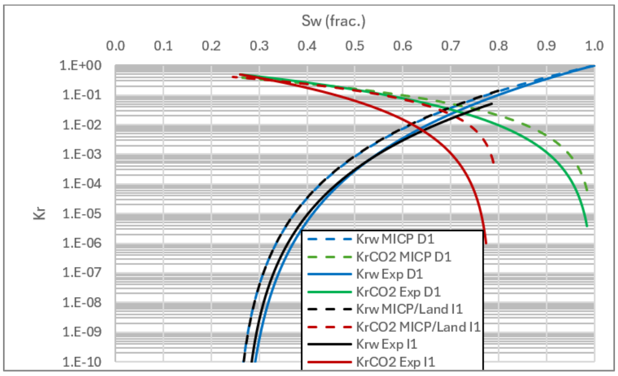

Fig. 18. Stack 1 Kr curves, indirect vs experimental.

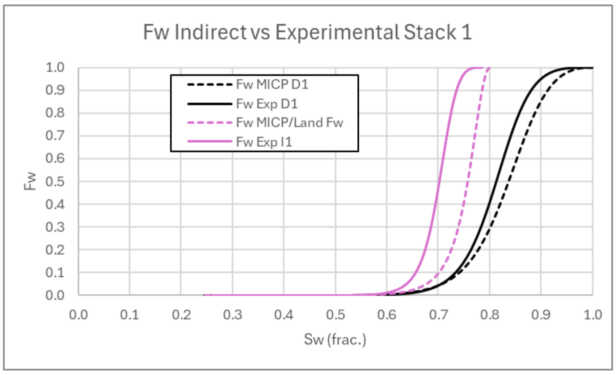

Fig. 19. Stack 1 fractional flow F_w curves, indirect vs experimental.

The results of the indirect approach for primary drainage are close to those from the experiment. It is less likely for the imbibition cycle: the observed differences are due to the high N_{CO_2} value from the experiment (2 times higher than N_{CO_2} from the indirect method).

Stack 2 vs MICP High Flow Unit:

Figures 20 and 21 show the comparison between the indirect and lab-measured K_r and fractional flow F_w curves for Stack 2.

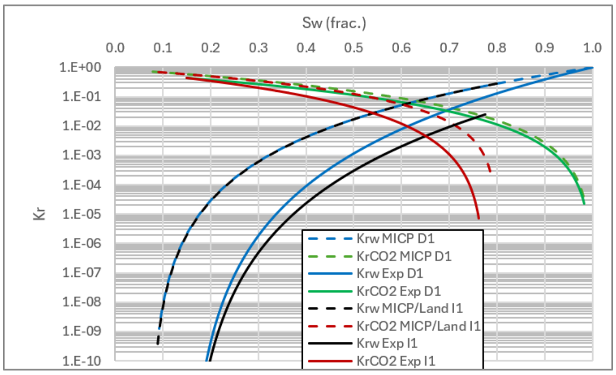

Fig. 20. Stack 2 K_r curves, indirect vs experimental.

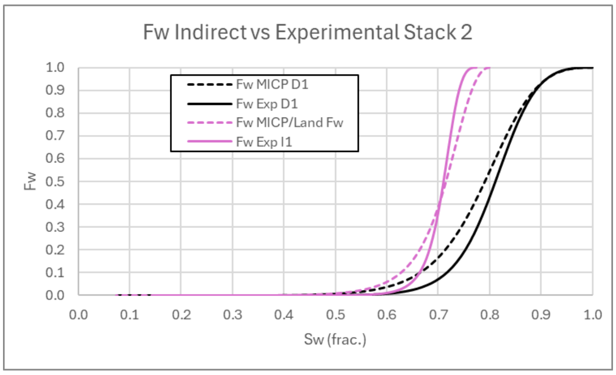

Fig. 21. Stack 2 fractional flow F_w curves, indirect vs experimental.

Figure 20 shows that the indirect and lab-measured K_r curves do not overlap. The main reasons are the low experimental K_{rg} Max and higher experimental S_{wi} compared to the same parameters indirectly obtained. Nevertheless, when looking at Figure 21, the fractional flow F_w curves of both primary drainage and imbibition cycles are close to each other.

Stack 3 vs MICP High Flow Unit:

Figures 22 and 23 show the comparison between the indirect and lab-measured K_r and fractional flow F_w curves for Stack 3.

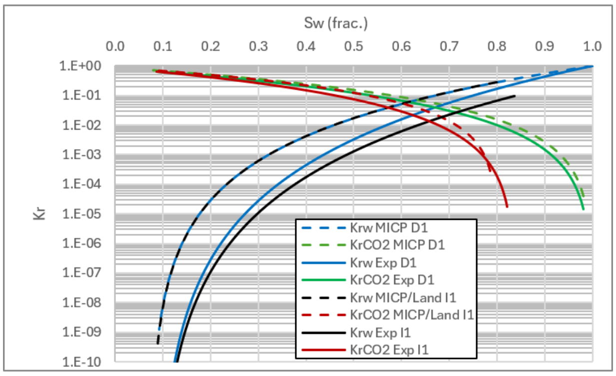

Fig. 22. Stack 3 K_r curves, indirect vs experimental.

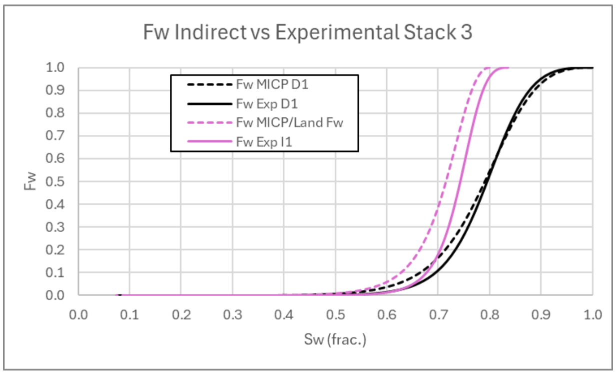

Fig. 23. Stack 3 fractional flow F_w curves, indirect vs experimental.

Except the difference between the indirect and lab-measured K_{rw} curves in Figure 22 (due to the difference in S_{wi} values), there is an acceptable agreement between the derived and experimental results for both primary drainage and imbibition cycles.

Based on the above observations, it is considered that the indirect Brooks-Corey approach based on MICP data provides a "good enough" inputs to perform simulations at reservoir scale when advanced SCAL coreflooding results are not yet available. It must be confirmed by comparing the simulations at the reservoir scale using the indirect and experimental interpreted K_r results: the derived MICP Kr cannot consider any interaction between rock mineralogy/CO_2 such as salts precipitation or rock brine interaction (which may affect Kr, injectivity, mobility, ...).

6 Dynamic Reservoir Simulations

The impact of synthetic and laboratory-measured K_r and P_c functions on CO_2 injection behaviour was evaluated through two dynamic reservoir simulation cases. In the first case, Brooks-Corey Kr and Pc curves derived from MICP data were applied, while the second case used laboratory measured SCAL curves. The static reservoir model was discretized using cartesian grid blocks with lateral dimensions of 500×500 ft and a vertical resolution of 4 ft. The model represents the data captured from the Stratigraphic well drilled for this project. No faults were identified within the modelled area of interest. All simulations were conducted using a compositional fluid model, with the injection stream represented as pure CO_2.

The development strategy imposed a constant CO_2 injection rate of 3,287 metric tons per day (equivalent to 1.2 million metric tons per year), with injection pressure constrained to remain below 90% of the estimated fracture initiation pressure. The injection period is 12 years, resulting in a total injected volume of 14.4 million metric tons of CO_2. The injection was completed over a 200 ft perforated interval within the target injection zone.

Figure 24 shows the resulting simulation at the end of the 12 years of injection using the Brooks-Corey Kr and Pc functions, while Figure 25 shows the resulting simulation at the end of 12 years of injection, but with the SCAL Kr and Pc functions.

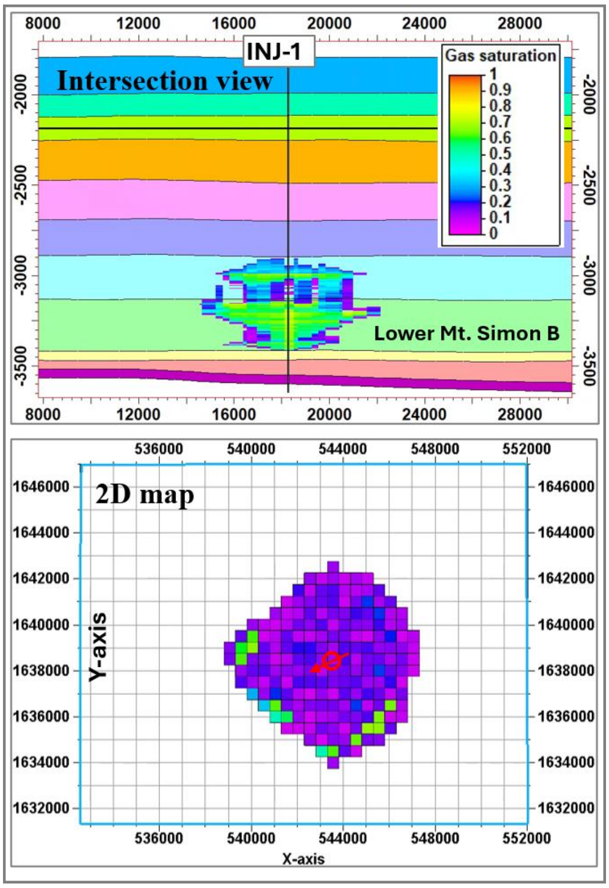

Fig. 24. Primary drainage simulation using indirect K_r and P_c.

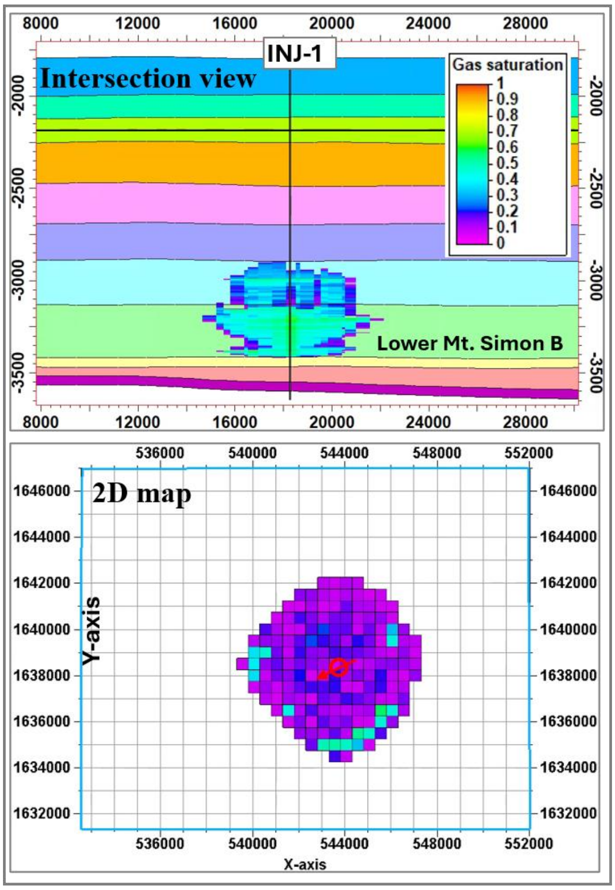

Fig. 25. Primary drainage simulation using experimental SCAL K_r and P_c, post-history-match.

Simulation outcomes demonstrate that the use of synthetic curves resulted in negligible deviation in plume behavior over the 12 years of injection period. The predicted CO_2 plume area is 1,018 acres for the synthetic-curve case compared with 934 acres for the SCAL-based case at the end of injection, representing a difference of 8 %. Figure 24 and Figure 25 illustrate CO_2 migration at the end of 12 years of injection through a 2D map view and an intersection plane (by zones). This deviation is within the expected uncertainty for permeability-dependent flow functions in saline-reservoir CO_2 storage models and supports the use of synthetic functions as a conservative, physically defensible representation of multiphase flow processes.

The analysis further confirms that when flow units are rigorously defined using measured primary drainage capillary pressure data, the Brooks–Corey formulation offers a robust and internally consistent framework for estimating drainage relative permeability. This approach reduces the dependency on extensive SCAL datasets while still preserving the dominant controls on CO_2 mobility and vertical migration height within the simulation model.

The imbibition cycle was also simulated: the objective was to observe the impact of the imbibition SCAL P_c on the simulations and confirm the findings made by [31]. Figure 26 represents the CO_2 plume (after 200 years) when the imbibition Pc is deactivated, while Figure 27 represents the CO_2 plume with the simulated SCAL P_c.

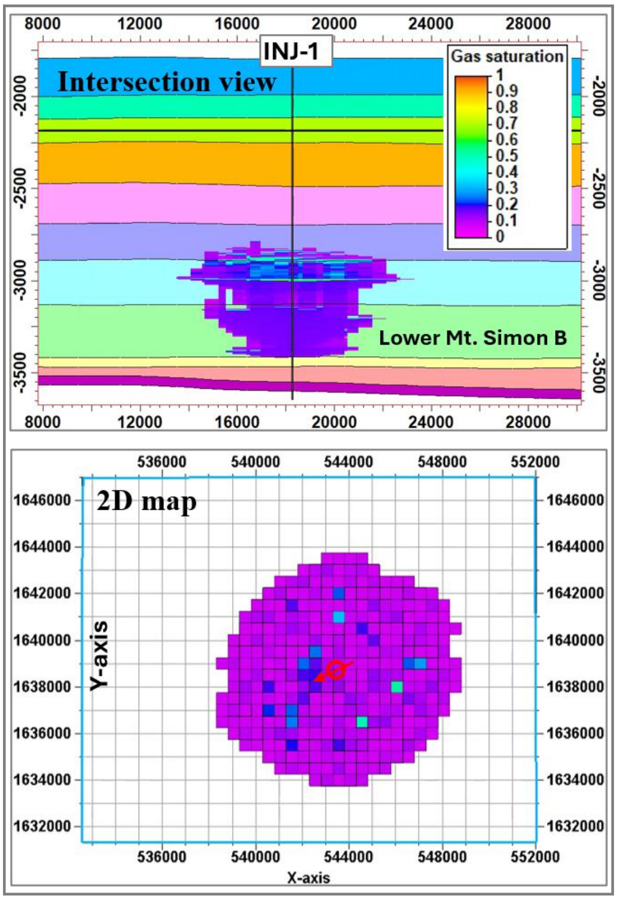

Fig. 26. Imbibition simulation with no imbibition P_c.

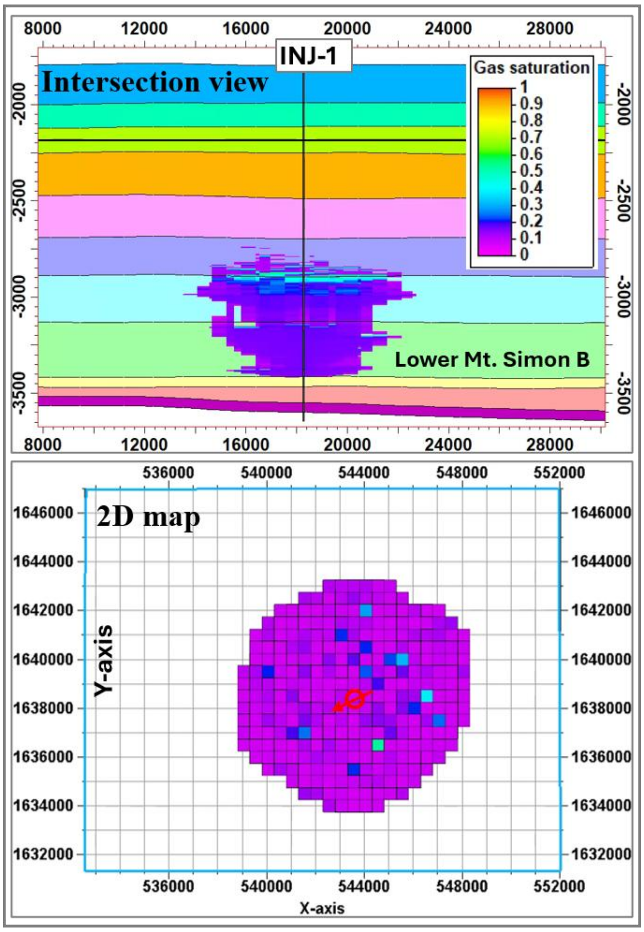

Fig. 27. Imbibition simulation with imbibition P_c.

When imbibition P_c behavior is omitted (by deactivating the imbibition capillary pressure curve during the hysteresis process in the dynamic simulation), the results indicate a minimal impact even on long-term CO_2 plume behavior. Over a 200-year post-injection period, this omission results in a slightly more laterally extensive and mobile CO_2 plume (1,769 acres versus 1,586 acres). However, the overall influence on CO_2 plume evolution remains modest, with differences within approximately 10%, consistent with trends reported in the study made by [31]. If the imbibition P_c>0 can be neglected in our case study, it may not always be the case: when the reservoirs contain layers with large permeability variations between layers, neglecting the positive imbibition Pc will result in no exchanges between the layers.

7 Conclusions

The study successfully demonstrates that the indirect Brooks-Corey approach, using Mercury Injection Capillary Pressure (MICP) and reservoir fluid properties, can provide a "sufficiently accurate" set of relative permeability K_r curves, for the given lithology and fluid system within a compressed period (less than two weeks).

In our case study, the results indicate that MICP-derived K_r curves are an acceptable proxy for estimating CO_2–brine relative permeability in primary drainage, showing close agreement with later experimental core flooding results. While the indirect method was less predictive for the imbibition cycle due to higher experimental N_{CO_2} values (lower CO_2 mobility), the impact on overall plume evolution in dynamic simulations remained modest. This methodology allows for the delivery of critical dynamic reservoir modeling data ahead of strict deadlines, such as the Class VI permit application in the United States. Comparative simulations showed that using indirect K_r curves resulted in only 8% difference in predicted CO_2 plume area compared to final SCAL-based cases, which falls within the expected uncertainty envelope for such models. Although incorporating imbibition capillary pressure better represents capillary driven CO_2 immobilization after injection, omitting it results in only a modest difference.

To conclude, the Fast-Track SCAL workflow (delivering data in less than two weeks) allowed the operator to meet Class VI permit deadlines with a "sufficiently accurate" dataset that preserves the dominant controls on CO_2 mobility and trapping efficiency.

Acknowledgments

The authors would like to thank SLB and Lapis Carbon Solutions for permission to publish this work.

References

1. Chen, C., *et al.*: “Characterization of CO_2-brine relative permeability and capillary pressure in Berea sandstone”, Water Resources Research, **50**, p. 7140–7161, 2014.
2. Chen, C., *et al.*: “Impact of capillary end effects on the measurement of CO_2-brine relative permeability”, International Journal of Greenhouse Gas Control, **49**, p. 115-126, 2016.
3. Bennion, D.B., Bachu, S.: “Relative Permeability Characteristics for Supercritical CO_2 Displacing Water in a Variety of Reservoir Formations in the Western Canadian Sedimentary Basin”, SPE-95547-MS, 2005.
4. Bennion, D.B., Bachu, S.: “Drainage and Imbibition Relative Permeability Relationships for Supercritical CO_2/Brine and H_2S/Brine Systems in Intergranular Sandstone and Carbonate Formations”, SPE-114482-MS, 2008.
5. Al-Yousef, A.S., *et al.*: “Relative permeability and wettability of the San Saba sandstone for CO_2 storage applications using NMR”, Fuel, 285, 119104, 2021.
6. Pini, R., *et al.*: “Capillary pressure and simultaneous measurement of relative permeability in the CO_2-water system”, Advances in Water Resources, **38**, p. 48-59, 2012.
7. Krevor, S.C., *et al.*: “Relative permeability and trapping of CO_2 in native rocks from regional systems”, International Journal of Greenhouse Gas Control, **7**, p. 115-129, 2012.
8. Burnside, N.M., Naylor, M.: “Review and implications of relative permeability of CO_2-brine

systems and residual trapping of CO_2", Internation Journal of Greenhouse Gas Control, **23**, p.1-11, 2014.

9. Ott, H., *et al.*: "Core-flood experiment for CO_2 storage: Comparison of relative permeability and capillary pressure with digital rock physics", SPE-154448-MS, 2012.
10. Akbarabadi, M., Piri, M.: "Relative permeability, hysteresis, and capillary trapping characteristics of supercritical CO_2/brine systems", Advances in Water Resources, **52**, p. 190–206, 2013.
11. Zuo, L., Benson, S.M., *et al.*: "Experimental study of CO_2-brine relative permeability and capillary pressure in reservoir rocks", Energy Procedia, **37**, p. 5600-5607, 2012.
12. Reynolds, C.A., Krevor, S.: "Characterizing flow heterogeneity in core-flood relative permeability measurements of CO_2 and brine in sandstone", Advances in Water Resources, **76**, p. 14–25, 2015.
13. Perrin, J.C., Benson, S.M.: "An experimental study on the influence of sub-core scale heterogeneities on CO_2 distribution in reservoir rocks", Transport in Porous Media, **82**, p. 93–109, 2010.
14. Shi, J.-Q., *et al.*: "CO_2-brine relative permeability measurements on a Paaratte formation sandstone core sample", Energy Procedia, **1)**, p. 3205-3212, 2009.
15. Motealleh, K., *et al.*: "Primary drainage relative permeability of CO_2/brine in Berea sandstone: Impact of flow rate and flow orientation", International Journal of Greenhouse Gas Control, **124**, 103858, 2023.
16. Mascle, M., *et al.*: "Relative permeability measurements for CO_2 storage: Impact of experimental conditions and interpretation methods", Petrophysics, **64**, 2023.
17. Munkerud, P.K., *et al.*: "Experimental Relative Permeability Studies for the Northern Lights Project", Energy Procedia/GHGT-16, 2023.
18. Pentland, C.H., *et al.*: "Measurement of non-wetting phase trapping in water-wet rocks", Water Resources Research, **47**, W08523, 2011.
19. Krevor, S.C., *et al.*: "Relative permeability and trapping of CO_2 in sandstone formations", Water Resources Research, **48**, W02532, 2012.
20. Land, C.S.: "Calculation of Imbibition Relative Permeability for Two- and Three-Phase Flow from Rock Properties", Society of Petroleum Engineers Journal, **8**, p. 149–156, 1968.
21. Niu, B., *et al.*: "The effect of temperature and pressure on coincident measurements of capacitance and relative permeability of CO_2 and brine", International Journal of Greenhouse Gas Control, **36**, p. 116–126, 2015.
22. Tanino, Y., Blunt, M.J.: "Capillary trapping of CO_2: Trapping characteristic curves for sandstones", Water Resources Research, **48**, W02515, 2012.
23. Iglauer, S., *et al.*: "Comparison of the influence of pore structure and wettability on capillary trapping in sandstones", Advances in Water Resources, **34**, p. 1365–1374, 2011.
24. Ruprecht, C., *et al.*: "Hysteretic Carbon Dioxide–Brine Relative Permeability in Berea Sandstone", SPE-169123-MS, 2014.
25. Acharya, S., *et al.*: "Effect of Injection Pressure on CO_2–Brine Relative Permeability in Low-Permeability Reservoirs", Energy & Fuels, **38**, 2024.
26. Brooks, R. H. and Corey, A. T.: "Properties of Porous Media Affecting Fluid Flow", J. Irrig. Drain. Div., 6, **61**, 1966.
27. Leverett, M.C.: "Capillary behavior in porous solids". Transactions of the AIME (142): 159–172, 1941.
28. Pairoys, F., Caubit, C.: "Water-gas imbibition relative permeability: Literature review, direct versus indirect methods and experimental recommendations", SCA2022-024, 2022.
29. Timur, A.: "An Investigation of Permeability, Porosity and Residual Water Saturation Relationship for Sandstone Reservoirs", The Log Analyst, 1968.
30. Langaas, K. *et al.*: "A criterion for ordering individuals in a composite core", Journal of Petroleum Science and Engineering, **19**, p. 21-32, 1998.
31. Lun, L.S and Gao, B.: "Developing Consistent Relative Permeability and Capillary Pressure Models for Reservoir Simulation of CCS Projects", SPE-216722-MS, 2023.